JOURNAL OF SPACECRAFT AND ROCKETS
Vol. 40, No. 2, March–April 2003

Optimum Thrust Pitch Profiles for Certain Orbit Control Problems

Jean A. Kéchichian*
The Aerospace Corporation, El Segundo, California 90245-4691

Optimal thrust pitch profiles that maximize the change in the semimajor axis while constraining the eccentricity change at zero over a revolution, in the presence of shadowing where no thrust is applied, are generated by using numerical quadrature methods. The procedure is extended to the dual problem of maximizing the change in eccentricity while constraining the semimajor axis change at zero for the near-circular case with shadowing. The method is further applied to the more general elliptic case using continuous thrust to circularize a highly elliptic synchronous orbit that stays synchronous during the circularization maneuver. For the simplified problem where the thrust is applied normal to the line of apsides, the use of the averaged rate of the eccentricity leads to an analytic expression relating the current eccentricity to the accumulated thrust time during the circularization. This expression allows for a quick evaluation of the required velocity change for a given initial elliptic orbit to circularize. Finally, for the near-circular case, the simultaneous circularization and orbit plane rotation using constant thrust yaw profile and inertially fixed in-plane thrust orientation, as in the simplified circularization problem, leads to an analytic expression for the required velocity change to effect a given orbit rotation with given initial eccentricity. The constant yaw angle needed for such a transfer is also obtained analytically.

Nomenclature

a	=	semimajor axis, km
E	=	eccentric anomaly
e	=	eccentricity
f_r, f_θ, f_h	=	radial, normal, and out-of-plane thrust acceleration, km/s^2
h	=	orbital angular momentum, km^2/s
i	=	orbit plane inclination
n	=	satellite orbit mean motion, rad/s
p	=	orbit parameter, $a(1-e^2)$, km
r	=	radial distance, km
$\hat{\boldsymbol{r}}$	=	unit vector in radial direction
$\boldsymbol{T}$	=	thrust acceleration vector
α	=	thrust pitch angle
Δa	=	change in semimajor axis, km
Δe	=	change in eccentricity
θ^*	=	true anomaly
μ	=	Earth gravity constant, km^3/s^2
ω	=	argument of perigee

Introduction

SEVERAL of the more fundamental orbit control laws using both impulsive and low-thrust propulsion modes have been summarized in Ref. 1, including the important optimal transfer problem between inclined circular orbits that lead to Edelbaum's closed-form expression for the total required velocity change that is widely used in the industry for rapid first-order evaluations. Cass, in Ref. 2, extended Edelbaum's analysis to the case of intermittent thrusting while still restricting himself to the circular assumption. Thus, the variable pitch angle is optimized in direction to keep the orbit circular despite the presence of a shadow arc along the orbit, while simultaneously minimizing the transfer time from the given initial orbit to the final destination orbit and carrying out the required orbit plane rotation in the process.

Received 5 June 2002; revision received 24 September 2002; accepted for publication 26 September 2002.

*Engineering Specialist, Astrodynamics Department, Mail Stop M4-947, P.O. Box 92957, Los Angeles, CA 90009; Jean.A.Kechichian@aero.org. Associate Fellow AIAA.

The theory of maxima is used instead of the calculus of variations to find the optimal pitch profile that maximizes the change in the semimajor axis while constraining the eccentricity change at zero over a revolution in circular orbit[1–3] for both the continuous and discontinuous thrust cases. This maximization technique is applied in this present paper to the dual problem of maximizing the change in eccentricity while constraining the semimajor axis change at zero for the near-circular case in the presence of shadowing. The method is then extended to the more general elliptic case in the continuous thrust case only, to circularize slowly a highly elliptic orbit without affecting its orbital energy. This particular example is presently used in the final steps of transferring certain communications satellites to their geosynchronous orbits after their proper placement in an intermediate elliptic synchronous orbit using chemical propulsion. The optimal thrust pitch profile in this continuous thrust case is found nearly to match the much simpler Spitzer[4,5] scheme, where the thrust vector is aligned normal to the orbit line of apsides such that it keeps an inertially fixed orientation in space and is implemented easily. When averaged rates of change of the eccentricity variable are used, analytic expressions that relate the current eccentricity to the accumulated thrust time as well as the required velocity change to circularize an initial elliptic orbit are easily obtained for the Spitzer scheme. When the perturbation in the true anomaly is neglected, the change in the eccentricity using Spitzer's suboptimal firing mode is carried out without affecting the orbit semimajor axis as desired. However, the optimal thrust profile is to be used instead in the discontinuous thrust case because then the semimajor axis cannot be kept constant as shown in the near-circular examples in this paper. In the near-circular case, Spitzer's in-plane firing strategy is easily combined with the orbit plane rotation using a constant out-of-plane thrust angle switched between its positive and negative values every one-half revolution, and analytic expressions for the out-of-plane thrust angle as well as the total required velocity change to circularize and rotate simultaneously the orbit plane are derived for rapid first-order evaluations in the continuous thrust transfer case.

Maximization of the Changes in Semimajor Axis and Eccentricity in Near-Circular Orbit in the Presence of a Shadow Arc

Let Fig. 1 represent a near-circular orbit whose perigee is at 0 and where no thrust is applied on the shadow arc 0′0. When θ^* is measured from the shadow exit point 0 and α from the direction $\hat{\boldsymbol{r}}$, the optimal α profile that maximizes Δa, while constraining Δe at zero after one thrust cycle along 00′, can be determined following the approach used in Ref. 2.

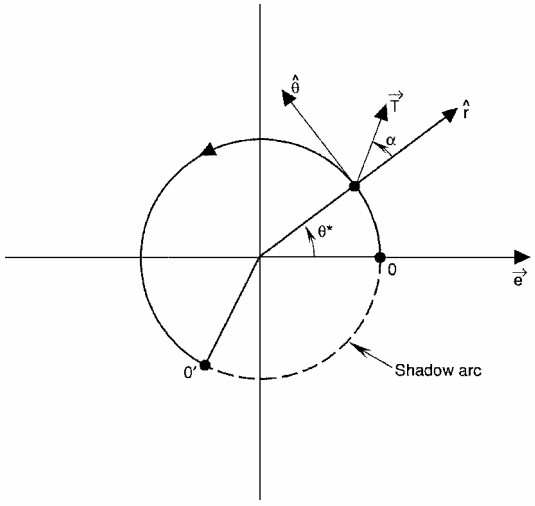

Fig. 1 Thrust geometry and shadow arc in near-circular orbit.

The variation of parameters equations in term of the acceleration components $f_r = kc_\alpha$ and $f_\theta = ks_\alpha$, where $k = \boldsymbol{T}$, are given by

$$\dot{a} = (2a^2/h)[es_{\theta^*} f_r + (p/r) f_\theta] \tag{1}$$

$$\dot{e} = (1/h)\{ps_{\theta^*} f_r + [(p+r)c_{\theta^*} + re] f_\theta\} \tag{2}$$

Here $s_{\theta^*} = \sin\theta^*$, $c_{\theta^*} = \cos\theta^*$, etc. These equations are readily converted to the form[2]

$$\dot{a} = \frac{2es_{\theta^*}}{n(1-e^2)^{\frac{1}{2}}} f_r + \frac{2(1+ec_{\theta^*})}{n(1-e^2)^{\frac{1}{2}}} f_\theta \tag{3}$$

$$\dot{e} = \frac{(1-e^2)^{\frac{1}{2}} s_{\theta^*}}{na} f_r + \frac{(1-e^2)^{\frac{1}{2}}}{nae}\left[1 + ec_{\theta^*} - \frac{1-e^2}{1+ec_{\theta^*}}\right] f_\theta \tag{4}$$

For near-circular orbits, these equations simplify after setting $e = 0$ to

$$\dot{a} = 2f_\theta/n \tag{5}$$

$$\dot{e} = (s_{\theta^*}/na) f_r + (2c_{\theta^*}/na) f_\theta \tag{6}$$

The changes in a and e over one cycle of thrust from $\theta^* = 0$ to τ_f or from 0 to $0'$ are given by

$$\Delta a = \frac{2ka^3}{\mu} \int_0^{\tau_f} s_\alpha \, \mathrm{d}\theta^* \tag{7}$$

$$\Delta e = \frac{ka^2}{\mu} \int_0^{\tau_f} (c_\alpha s_{\theta^*} + 2s_\alpha c_{\theta^*}) \, \mathrm{d}\theta^* \tag{8}$$

The maximization of Δa subject to $\Delta e = 0$ is made possible by adjoining the constraint $\Delta e = 0$ to Δa by way of a constant Lagrange multiplier λ such that the performance index is given by

$$I(\alpha) = \int_0^{\tau_f} \left\{ \frac{ka^2}{\mu} [2as_\alpha + \lambda(c_\alpha s_{\theta^*} + 2s_\alpha c_{\theta^*})] \right\} \mathrm{d}\theta^* \tag{9}$$

Letting F represent the integrand of the preceding integral and applying Euler's condition $\partial F/\partial\alpha = 0$ will yield the optimal α equation as

$$\tan\alpha = \frac{2(a + \lambda c_{\theta^*})}{\lambda s_{\theta^*}} \tag{10}$$

such that

$$s_\alpha^2 = \frac{4(a+\lambda c_{\theta^*})^2}{\lambda^2 s_{\theta^*}^2 + 4(a+\lambda c_{\theta^*})^2}, \qquad c_\alpha^2 = \frac{\lambda^2 s_{\theta^*}^2}{\lambda^2 s_{\theta^*}^2 + 4(a+\lambda c_{\theta^*})^2}$$

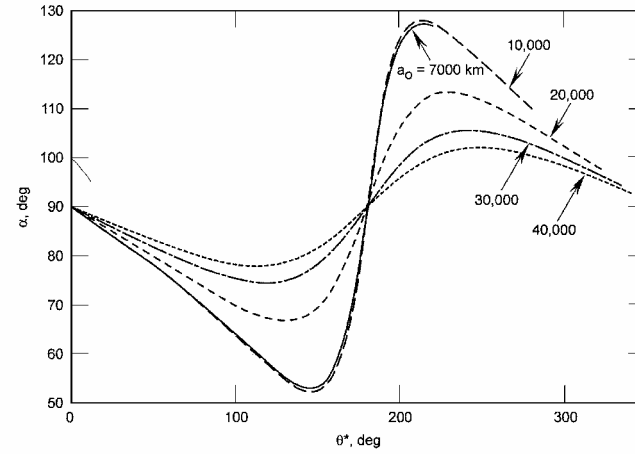

Fig. 2 Optimal pitch profiles for constrained maximum Δa with worst-case shadowing in circular orbit.

Inserting s_α and c_α in the Δe expression in Eq. (8) yields

$$\Delta e = \frac{ka^2}{\mu} \int_0^{\tau_f} \frac{\left(4ac_{\theta^*} + \lambda + 3\lambda c_{\theta^*}^2\right)}{\left[4a^2 + 4a\lambda c_{\theta^*} + \lambda\left(\lambda + 3\lambda c_{\theta^*}^2 + 4ac_{\theta^*}\right)\right]^{\frac{1}{2}}} \mathrm{d}\theta^* \tag{11}$$

where λ is determined numerically by way of a 10-point Gauss–Legendre quadrature of the preceding integral and its value adjusted slowly until $\Delta e = 0$ is satisfied to within a certain tolerance. The thrust pitch profile is then obtained from Eq. (10) and the maximum change in Δa from Eq. (7) by numerical quadrature. Figure 2 shows the optimal pitch profiles for $a = 7000$-, 10,000-, 20,000-, 30,000-, and 40,000-km cases using $k = 3.5 \times 10^{-7}$ km/s^2, as a function of θ^* and for the maximum shadow arc length encountered by each circular orbit size. These arcs are such that $\tau_f = 220, 280, 322, 335$, and 341 deg, respectively. These profiles start at $\alpha = 90$ deg, which is also the value for $\theta^* = 180$ deg resulting in the pinch point shown in Fig. 2.

The maximization of Δe subject to $\Delta a = 0$ is carried out by forming the dual performance index:

$$I(\alpha) = \int_0^{\tau_f} \left\{ \frac{ka^2}{\mu} [(c_\alpha s_{\theta^*} + 2s_\alpha c_{\theta^*}) + \lambda(2as_\alpha)] \right\} \mathrm{d}\theta^* \tag{12}$$

Let F represent now the new integrand; the Euler equation $\partial F/\partial\alpha = 0$ leads to the solution

$$\tan\alpha = 2(c_{\theta^*} + a\lambda)/s_{\theta^*} \tag{13}$$

such that

$$s_\alpha^2 = \frac{4(c_{\theta^*} + a\lambda)^2}{s_{\theta^*}^2 + 4(c_{\theta^*} + a\lambda)^2}$$

$$c_\alpha^2 = \frac{s_{\theta^*}^2}{s_{\theta^*}^2 + 4(c_{\theta^*} + a\lambda)^2}$$

Inserting s_α in Eq. (7) for Δa yields

$$\Delta a = 2k\frac{a^3}{\mu} \int_0^{\tau_f} \frac{2(c_{\theta^*} + a\lambda)}{\left[1 + 3c_{\theta^*}^2 + 4a\lambda(a\lambda + 2c_{\theta^*})\right]^{\frac{1}{2}}} \mathrm{d}\theta^* = 0 \tag{14}$$

As before, λ is determined numerically by adjusting its value until the numerical quadrature of the preceding integral yields a value of zero to within a small tolerance. Δe is then computed by quadrature using the s_α, c_α, and λ values of the optimal solution in Eq. (8). Figure 3 shows the optimal pitch profile for the same five cases, namely, $a = 7000$, 10,000, 20,000, 30,000, and 40,000 km with maximum shadow arcs, as a function of θ^*. The varying angle α starts at $\alpha = 90$ deg and crosses the -90-deg value at $\theta^* = 180$ deg,

Table 1 Iterated and integrated multiplier and orbit parameters

Parameter	Values				
a, km	7,000	10,000	20,000	30,000	40,000
τ_f, deg	220	280	322	335	341
δ, deg	140	80	38	25	19
$\lambda_{\Delta a}$	5,823.049823	8,379.265958	13,034.177567	14,569.241955	15,548.465162
$\lambda_{\Delta e}$	0.513697×10^{-4}	0.359287×10^{-4}	0.87259×10^{-5}	0.39454×10^{-5}	0.23495×10^{-5}
Δa (optimal), km	2.107	7.660	75.856	272.102	661.563
Δe (optimal)	0.254313×10^{-3}	0.615390×10^{-3}	0.292109×10^{-2}	0.694068×10^{-2}	0.1264526×10^{-1}
$(a_f)_{\Delta a}$, km	7,002.107	10,007.729	20,075.778	30,272.105	40,661.574
$(a_f)_{\Delta e}$, km	7,000.001	10,000.017	19,999.645	29,999.601	40,000.778
$(e_f)_{\Delta a}$	5.799×10^{-8}	9.113×10^{-6}	6.808×10^{-6}	3.229×10^{-7}	9.045×10^{-7}
$(e_f)_{\Delta e}$	2.542205×10^{-4}	6.149686×10^{-4}	2.923213×10^{-3}	6.943196×10^{-3}	1.264781×10^{-2}

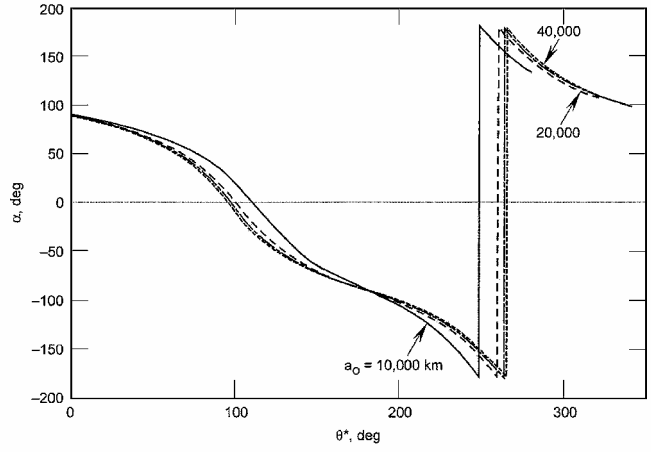

Fig. 3 Optimal pitch profiles for constrained maximum Δe with worst-case shadowing in circular orbit.

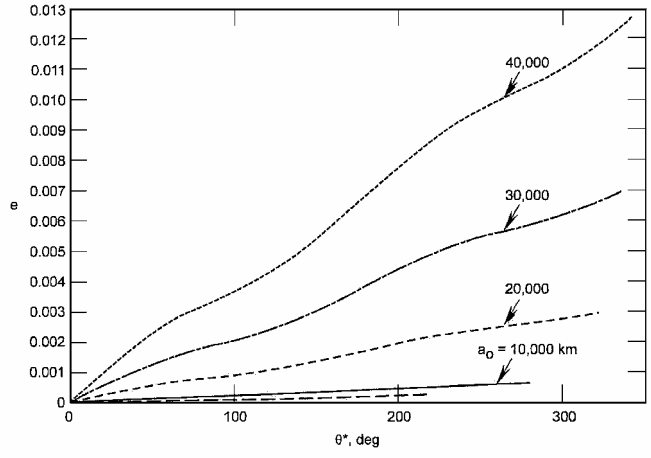

Fig. 4 Eccentricity variation for constrained maximum Δe solutions with worst-case shadowing in circular orbit.

resulting in another pinch point as shown in Fig. 3. The eccentricity history is obtained by integrating Eq. (6) for $\dot{e}$ with a change of the independent variable from time t to θ^* such that

$$\frac{\mathrm{d}e}{\mathrm{d}\theta^*} = \frac{ka^2}{\mu}(c_\alpha s_{\theta^*} + 2s_\alpha c_{\theta^*}) \tag{15}$$

In a similar way, $\dot{a}$ in Eq. (5) is transformed to

$$\frac{\mathrm{d}a}{\mathrm{d}\theta^*} = 2k\frac{a^3}{\mu}s_\alpha \tag{16}$$

using $\mathrm{d}\theta^*/\mathrm{d}t = n$. When a is held as a constant outside the integration sign, the evolution of e for the five cases considered is shown in Fig. 4.

In Table 1, δ is the total maximum shadow angle that takes places when the sun–Earth line is contained in the spacecraft orbit plane, and $\lambda_{\Delta a}$ and $\lambda_{\Delta e}$ are the iterated values of λ for the Δa and Δe maximization cases, respectively. Δa (optimal) and Δe (optimal) are the corresponding optimal values of Δa and Δe obtained by numerical quadrature of the integrals in Eqs. (7) and (8). The final or achieved values of a and e for the two optimization problems are obtained from the integration of Eqs. (16) and (15). When Δe is maximized, $(a_f)_{\Delta e}$ very closely matches the values of the initial semimajor axes in all five cases, whereas when Δa is maximized instead, $(e_f)_{\Delta a}$ is effectively very small near the zero value as desired. Here $\lambda_{\Delta a}$ is of the order of 10^4 in kilometers and $\lambda_{\Delta e}$ is of the order of 10^{-4} per kilometer.

For continuous thrust over the entire orbit without any shadow arc, the $a = 7000$ km orbit example yields $\lambda_{\Delta a} = 0.155565\times10^{-2}$ resulting in a flat α profile at 90 deg with $(e_f)_{\Delta a} = 1.5019\times10^{-11}$, which is effectively zero. When Δe is maximized instead, $\lambda_{\Delta e} = 0.185146\times10^{-5}$ resulting in $(a_f)_{\Delta e} = 7000.028$ km effectively constraining Δa at zero at the end of one cycle of thrust, with the α profile closely matching the theoretical profile $\tan\alpha = 2/\tan\theta^*$ of Ref. 1. In both optimization cases, λ must be equal to zero leading to $\alpha = 90$ deg constant for the Δa maximization case and $\tan\alpha = 2/\tan\theta^*$ for the Δe maximization case. In the latter case, the total Δe change is given analytically by a complete elliptic integral[1]

$$\Delta e = \frac{8k}{n^2a}\int_0^{\pi/2}\sqrt{1-\frac{3}{4}s^2_{\theta^*}}\,\mathrm{d}\theta^*, \qquad \Delta e = \frac{8\times1.2111k}{n^2a}$$

which corresponds to a ΔV of

$$\Delta V = 0.649V\Delta e$$

which is directly a function of the orbit semimajor axis and the thrust acceleration.

Spitzer Strategy

Spitzer proposed in the mid-1990s in Refs. 4 and 5 to use a combination of chemical and electric propulsion schemes to transfer a spacecraft to the geosynchronous orbit. The final phase of the transfer consists of applying a low-thrust acceleration in an inertially fixed orientation, which would be orthogonal to the line of apsides such that a synchronous eccentric orbit is slowly circularized at a constant energy level. In this scheme, the pitch angle α is equal to $\pi/2$-θ^* such that the α profile is not too different from the optimal law $\tan\alpha = 2/\tan\theta^*$. When $s_\alpha = c_{\theta^*}$ and $c_\alpha = s_{\theta^*}$ are used in Eqs. (15) and (16), which are then integrated from $\theta^* = 0$ to τ_f, the linear α profile as well as the a, e, and θ^* histories are plotted against those corresponding to the constrained Δa and Δe maximization solutions in Figs. 5–7. The Spitzer strategy yields $(e_f)_s = 2.584017\times10^{-4}$, which is slightly higher than $(e_f)_{\Delta e} = 2.542205\times10^{-4}$ obtained from the maximum Δe constrained solutions. However, unlike the constrained case, which effectively keeps the semimajor axis unchanged after the thrust cycle at $a_f = 7000.001$ km, the Spitzer program yields $(a_f)_s = 6999.612$ km. The Spitzer and maximum Δe α profiles cross at $\theta^* = 180$ deg with $\alpha = -90$ deg exactly in both cases as shown in Fig. 5. If $\alpha = 3\pi/2 - \theta^*$ is used instead in the Spitzer case, which is equivalent to saying that the thrust direction is 180 deg away from the inertially fixed orientation used earlier, namely, $\alpha = \pi/2 - \theta^*$,

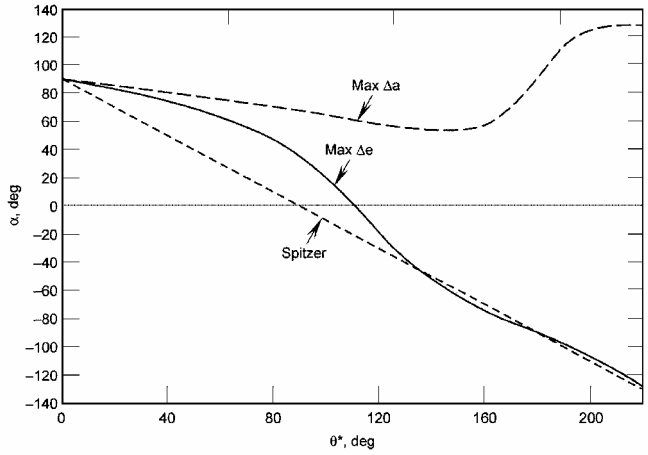

Fig. 5 Thrust pitch angle profiles for maximum Δe, maximum Δa, and Spitzer[4,5] solutions for $a_0 = 7000$ km circular orbit with worst-case shadowing.

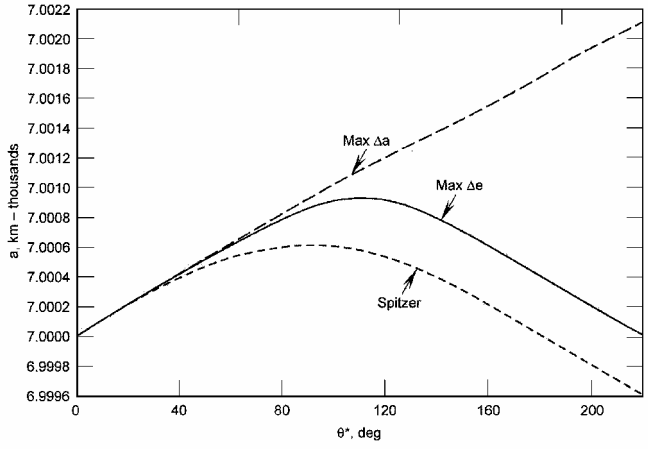

Fig. 6 Semimajor axis variation for maximum Δe, maximum Δa, and Spitzer[4,5] solutions for $a_0 = 7000$ km circular orbit with worst-case shadowing.

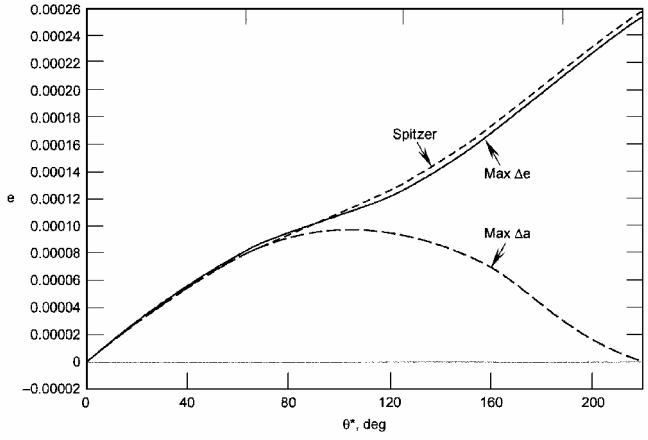

Fig. 7 Eccentricity variation for maximum Δe, maximum Δa, and Spitzer[4,5] solutions for $a_0 = 7000$ km circular orbit with worst-case shadowing.

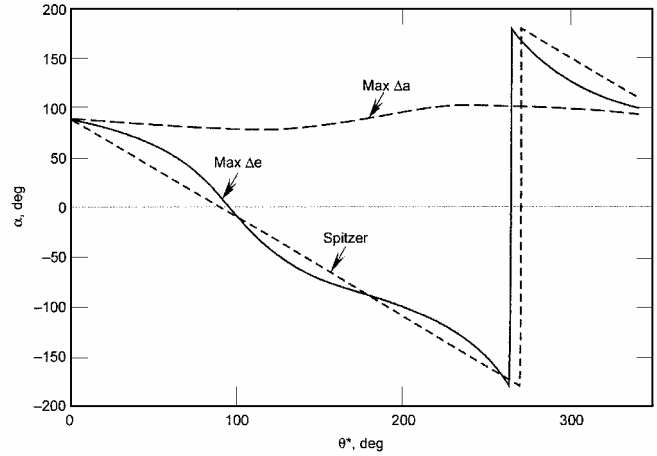

Fig. 8 Thrust pitch angle profiles for maximum Δe, maximum Δa, and Spitzer[4,5] solutions for $a_0 = 40{,}000$ km circular orbit with worst-case shadowing.

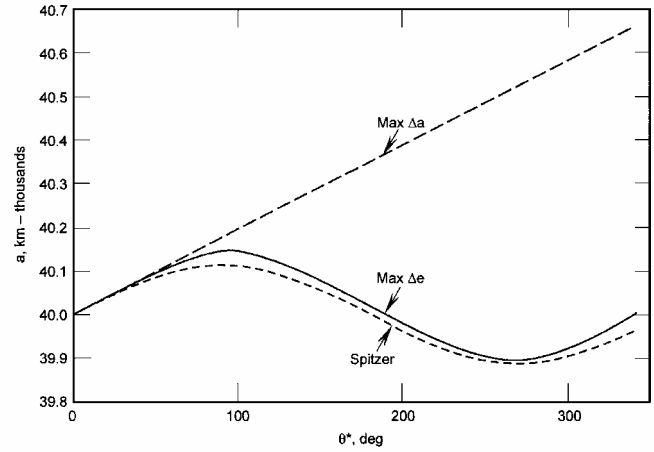

Fig. 9 Semimajor axis variation for maximum Δe, maximum Δa, and Spitzer[4,5] solutions for $a_0 = 40{,}000$ km circular orbit with worst-case shadowing.

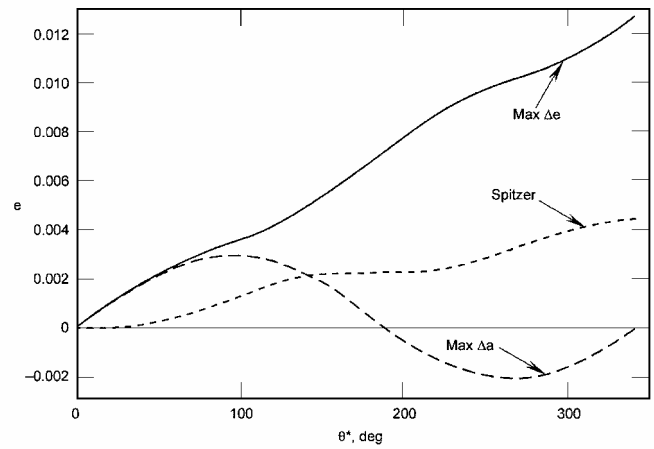

Fig. 10 Eccentricity variation for maximum Δe, maximum Δa, and Spitzer[4,5] solutions for $a_0 = 40{,}000$ km circular orbit with worst-case shadowing.

then the final semimajor axis $(a_f)_s = 7000.387$ km will be higher than the initial 7000-km value instead of being lower as earlier.

Figures 8–10 show the α and a and e variations of the Spitzer and the two optimized schemes for the $a = 40{,}000$ km case with $\tau_f = 341$ deg, or the maximum shadow condition. The angle $\alpha = \pi/2 - \theta^*$ is used for the Spitzer case, which yields $(a_f)_s = 39{,}963.408$ km and $(e_f)_s = 4.396957 \times 10^{-3}$, as opposed to $(a_f)_{\Delta e} = 40{,}000.778$ km and $(e_f)_{\Delta e} = 1.2647811 \times 10^{-2}$ of the constrained max Δe case, which yields the larger eccentricity change while satisfying the $\Delta a = 0$ constraint. Because of the larger values in the eccentricity experienced by thrusting in this larger orbit case, a modified form of Eqs. (3) and (4) is used because the circular orbit assumption that lead to Eqs. (15) and (16) used so far in the integrations is not fully valid anymore. Equations (3) and (4) are written with θ^* as the independent variable instead of time by neglecting the terms in f_r and f_θ in

$$\frac{\mathrm{d}\theta^*}{\mathrm{d}t} = \frac{h}{r^2} - \frac{r}{he}[-c_{\theta^*}(1 + ec_{\theta^*})f_r + s_{\theta^*}(2 + ec_{\theta^*})f_\theta]$$

such that

$$\frac{\mathrm{d}\theta^*}{\mathrm{d}t} = \frac{h}{r^2} = \frac{n(1+ec_{\theta^*})^2}{(1-e^2)^{\frac{3}{2}}} \tag{17}$$

where $h^2 = \mu a(1-e^2)$ and $r = a(1-e^2)/(1+ec_{\theta^*})$ are used. Equations (3) and (4) convert then to the form

$$\frac{\mathrm{d}a}{\mathrm{d}\theta^*} = \frac{2es_{\theta^*}(1-e^2)}{n^2(1+ec_{\theta^*})^2}kc_\alpha + \frac{2(1-e^2)}{n^2(1+ec_{\theta^*})^2}ks_\alpha + \frac{2(1-e^2)}{n^2(1+ec_{\theta^*})}ks_\alpha \tag{18}$$

$$\frac{\mathrm{d}e}{\mathrm{d}\theta^*} = \frac{(1-e^2)^2 s_{\theta^*}}{n^2 a(1+ec_{\theta^*})^2}kc_\alpha + \frac{(1-e^2)^2}{n^2 ae}\left[\frac{1}{(1+ec_{\theta^*})} - \frac{(1-e^2)}{(1+ec_{\theta^*})^3}\right]ks_\alpha \tag{19}$$

They are integrated numerically to produce the a and e evolutions in Figs. 9 and 10.

As a final note, if $\alpha = 3\pi/2 - \theta^*$ is used instead of $\alpha = \pi/2 - \theta^*$ for the Spitzer[4,5] case, the $(a_f)_s = 40{,}036.591\,\mathrm{km}$ is achieved instead of the 39,963.408 km value, indicating that semimajor axis increases in one case and decreases in the other. The change in eccentricity stays the same, but the location of the final perigee is different.

Incidentally, Eq. (16) in the circular case can be integrated analytically between $\theta^* = 0$ and θ^* yielding

$$a = a_0\left[1 - 4\left(ka_0^2/\mu\right)s_{\theta^*}\right]^{-\frac{1}{2}} \tag{20}$$

where a_0 is the initial semimajor axis. Equation (15) is easily integrated if a is held constant in the right-hand side such that

$$e = e_0 + (ka^2/\mu)\left[\tfrac{3}{2}\theta^* + s_{2\theta^*}\right] \tag{21}$$

Holding a as constant in the right-hand side of Eq. (16) results in the approximation $a = a_0 + 2k(a^3/\mu)s_{\theta^*}$. Equation (20) is exact, but e here is an approximation, and $e_0 = 0$ at the initial time. These examples show that important errors are associated with the use of the Spitzer[4,5] strategy when the thrust is off on the shadow arc as in solar electric applications.

Continuous Thrust Elliptic Case

Equations (3) and (4) valid in elliptic orbit can be written in terms of E as in Ref. 6 by using

$$\dot{E} = \left(\frac{\mu}{a}\right)^{\frac{1}{2}}\frac{1}{r} + \frac{1}{es_E}\left(c_E\frac{\mathrm{d}e}{\mathrm{d}t} - \frac{r}{a^2}\frac{\mathrm{d}a}{\mathrm{d}t}\right)$$

and by neglecting the $\mathrm{d}e/\mathrm{d}t$ and $\mathrm{d}a/\mathrm{d}t$ contributions such that

$$\dot{E} = (1/r)(\mu/a)^{\frac{1}{2}} \tag{22}$$

Also when the following identities are used,

$$s_{\theta^*} = \frac{(1-e^2)^{\frac{1}{2}}s_E}{(1-ec_E)}, \qquad c_{\theta^*} = \frac{c_E - e}{(1-ec_E)}$$

$$r = \frac{p}{(1+ec_{\theta^*})} = a(1-ec_E), \qquad p = a(1-e^2)$$

Eqs. (3) and (4) are transformed to the form after setting $f_r = ks_{\theta^*}$ and $f_\theta = kc_{\theta^*}$, that is, the Spitzer[4,5] mode

$$\frac{\mathrm{d}a}{\mathrm{d}E} = \frac{\mathrm{d}a}{\mathrm{d}t}\Big/\frac{\mathrm{d}E}{\mathrm{d}t}, \qquad \frac{\mathrm{d}a}{\mathrm{d}E} = \frac{2a^{\frac{7}{2}}}{\mu(p)^{\frac{1}{2}}}k(1-e^2)c_E \tag{23}$$

$$\frac{\mathrm{d}e}{\mathrm{d}E} = \frac{(p)^{\frac{1}{2}}}{\mu}a^{\frac{3}{2}}k\left(1 - 2ec_E + c_E^2\right) \tag{24}$$

The change in a after one full cycle of thrust between $E = 0$ and 2π is

$$\Delta a = \int_{a_0}^{a}\mathrm{d}a = \frac{2a^{\frac{7}{2}}}{\mu(p)^{\frac{1}{2}}}k(1-e^2)\int_0^{2\pi}c_E\,\mathrm{d}E = 0 \tag{25}$$

with a and e held constant in the right-hand side.

For the eccentricity change,

$$\Delta e = \int_0^e \mathrm{d}e = \frac{\left(p^{\frac{1}{2}}\right)}{\mu}a^{\frac{3}{2}}k\int_0^{2\pi}\left(1 - 2ec_E + c_E^2\right)\mathrm{d}E$$

$$\Delta e = 3\pi k a^{\frac{3}{2}}\frac{(p)^{\frac{1}{2}}}{\mu} \tag{26}$$

An average rate $(\widetilde{\mathrm{d}e}/\mathrm{d}t)$ can be produced from $\Delta e/\Delta \boldsymbol{T}$, where $\Delta \boldsymbol{T} = 2\pi/n$ is the orbit period with $n = \mu^{1/2}a^{-3/2}$ such that

$$\left(\frac{\widetilde{\mathrm{d}e}}{\mathrm{d}t}\right) = \frac{\Delta e}{\Delta \boldsymbol{T}} = \frac{3}{2}k\left(\frac{p}{\mu}\right)^{\frac{1}{2}} \tag{27}$$

This expression is integrated:

$$\int_{e_0}^{e}\frac{\mathrm{d}e}{\sqrt{1-e^2}} = \frac{3}{2}\frac{k}{\mu^{\frac{1}{2}}}a^{\frac{1}{2}}\int_0^t \mathrm{d}t$$

yielding

$$\sin^{-1}e - \sin^{-1}e_0 = \tfrac{3}{2}\left(k/\mu^{\frac{1}{2}}\right)a^{\frac{1}{2}}t_f \tag{28}$$

where t_f is now the total transfer time. The required ΔV to change the eccentricity from e_0 to e is then given by

$$\Delta V = kt_f = \tfrac{2}{3}(\mu/a)^{\frac{1}{2}}[\sin^{-1}e - \sin^{-1}e_0] \tag{29}$$

The optimal pitch profile for this continuous thrust elliptic case is obtained from Eqs. (18) and (19) for $(\mathrm{d}a/\mathrm{d}\theta^*)$ and $(\mathrm{d}e/\mathrm{d}\theta^*)$ valid in elliptic orbit. Holding a and e constant in these two equations and integrating with respect to θ^* from 0 to 2π yields the changes in Δa and Δe as

$$\Delta a = \frac{2(1-e^2)k}{n^2}\int_0^{2\pi}\left[\frac{es_{\theta^*}c_\alpha}{(1+ec_{\theta^*})^2} + \frac{s_\alpha}{(1+ec_{\theta^*})}\right]\mathrm{d}\theta^* \tag{30}$$

$$\Delta e = \frac{(1-e^2)^2 k}{n^2 a}\int_0^{2\pi}\left[\frac{s_{\theta^*}c_\alpha}{(1+ec_{\theta^*})^2} + \frac{s_\alpha}{e(1+ec_{\theta^*})} - \frac{(1-e^2)s_\alpha}{e(1+ec_{\theta^*})^3}\right]\mathrm{d}\theta^* \tag{31}$$

The maximization of Δe subject to the constraint $\Delta a = 0$ leads to the following performance index:

$$I(\alpha) = \frac{(1-e^2)^2 k}{n^2 a}\int_0^{2\pi}\left[\frac{s_{\theta^*}c_\alpha}{(1+ec_{\theta^*})^2} + \frac{s_\alpha}{e(1+ec_{\theta^*})} - \frac{(1-e^2)s_\alpha}{e(1+ec_{\theta^*})^3}\right]\mathrm{d}\theta^* + \lambda\frac{2(1-e^2)k}{n^2} \times \int_0^{2\pi}\left[\frac{es_{\theta^*}c_\alpha}{(1+ec_{\theta^*})^2} + \frac{s_\alpha}{(1+ec_{\theta^*})}\right]\mathrm{d}\theta^*$$

or

$$I(\alpha) = \frac{(1-e^2)k}{n^2}\int_0^{2\pi}\left\{\frac{(1-e^2)}{a}\left[\frac{s_{\theta^*}c_\alpha}{(1+ec_{\theta^*})^2} + \frac{s_\alpha}{e(1+ec_{\theta^*})} - \frac{(1-e^2)s_\alpha}{e(1+ec_{\theta^*})^3}\right] + 2\lambda\left[\frac{es_{\theta^*}c_\alpha}{(1+ec_{\theta^*})^2} + \frac{s_\alpha}{(1+ec_{\theta^*})}\right]\right\}\mathrm{d}\theta^* \tag{32}$$

Letting F represent the integrand, the optimal angle α is obtained from Euler's equation $\partial F/\partial\alpha = 0$, which results in

$$\tan\alpha = \frac{-(1-e^2)\left[(1+ec_{\theta^*})^2-(1-e^2)\right]-2ae\lambda(1+ec_{\theta^*})^2}{e(1+ec_{\theta^*})\left[-(1-e^2)s_{\theta^*}-2ae\lambda s_{\theta^*}\right]} \tag{33}$$

This expression yields in turn

$$s_\alpha^2 = \left\{-(1-e^2)\left[(1+ec_{\theta^*})^2-(1-e^2)\right]-2ae\lambda((1+ec_{\theta^*})^2\right\}^2/K$$

$$c_\alpha^2 = e^2(1+ec_{\theta^*})^2\left[-(1-e^2)s_{\theta^*}-2ae\lambda s_{\theta^*}\right]^2/K$$

where K is given by

$$K = e^2(1+ec_{\theta^*})^2\left[-(1-e^2)s_{\theta^*}-2ae\lambda s_{\theta^*}\right]^2 + \left\{-(1-e^2)\left[(1+ec_{\theta^*})^2-(1-e^2)\right]-2ae\lambda(1+ec_{\theta^*})^2\right\}^2$$

Using these s_α and c_α expressions in Eq. (30), the Δa integral effectively will be written in terms of θ^* after some minor manipulations as

$$\Delta a = \frac{2(1-e^2)k}{n^2} \times \int_0^{2\pi} \frac{[-(1-e^2)-2ae\lambda]\left(1+e^2+2ec_{\theta^*}\right)+(1-e^2)^2}{(1+ec_{\theta^*})K^{\frac{1}{2}}}\,\mathrm{d}\theta^* = 0 \tag{34}$$

K itself being a function of the constant λ, the latter multiplier's value is determined numerically using a search method until the preceding quadrature is effectively driven to zero to within a small tolerance. Once λ is thus determined, the achieved Δe change is also obtained by numerical quadrature using expression (31). When $a = 40{,}000$ km and $e = 0.7$ with $k = 3.5\times10^{-7}$ km/s^2 is used as an example, λ is found as $\lambda = -0.1669322321\times10^{-5}$ with corresponding $\Delta e = -0.87672449\times10^{-2}$ from the integral in Eq. (31). The integration of Eqs. (18) and (19) for $(\mathrm{d}a/\mathrm{d}\theta^*)$ and $(\mathrm{d}e/\mathrm{d}\theta^*)$ using the optimal control law of Eq. (33) yields $a_f = 40{,}004.722$ km, $e_f = 0.690371244$, or $\Delta e = 0.7 - e_f = 0.96287557\times10^{-2}$, which is slightly larger than the value obtained from the analytic form of Eq. (26) valid for the Spitzer[4,5] firing scheme, which reads as $\Delta e = 0.945595\times10^{-2}$. If $\alpha = 3\pi/2 - \theta^*$ is used to generate the numerically integrated Spitzer trajectory using Eqs. (18) and (19) by holding a and e as constants in the right-hand sides of these two differential equations, then the achieved a_f and e_f at $\theta^* = 360$ deg are obtained as 40,000.000 km and 0.6905440421, which corresponds to $\Delta e = 0.945595\times10^{-2}$, exactly the value from the analytic formula. There is practically no advantage in letting a and e vary in the right-hand sides of Eqs. (18) and (19) for this very low-thrust acceleration level especially that the perturbation in θ^* is neglected and the integration is essentially carried out along the initial conic.

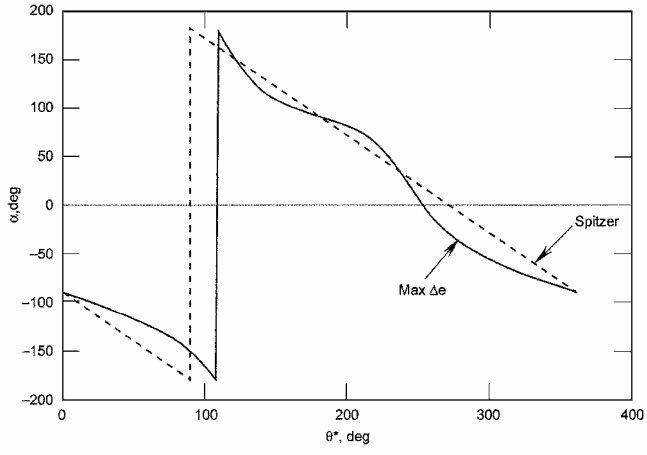

Fig. 11 Thrust pitch angle profiles for maximum Δe and Spitzer[4,5] solutions for $a_0 = 40{,}000$ km and $e_0 = 0.7$ elliptic orbit without shadow arc.

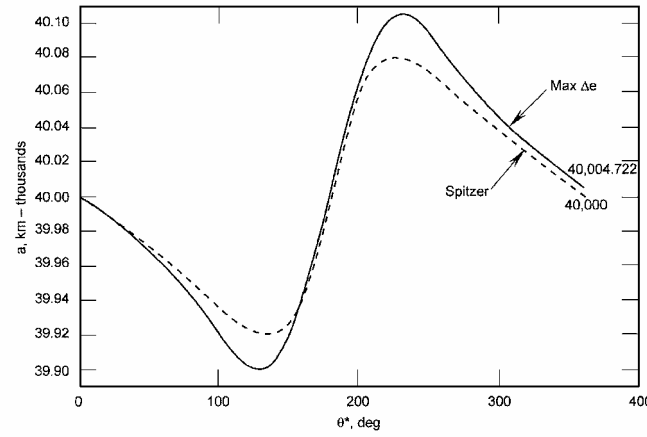

Fig. 12 Semimajor axis variation for maximum Δe and Spitzer[4,5] solutions for $a_0 = 40{,}000$ km and $e_0 = 0.7$ elliptic orbit without shadow arc.

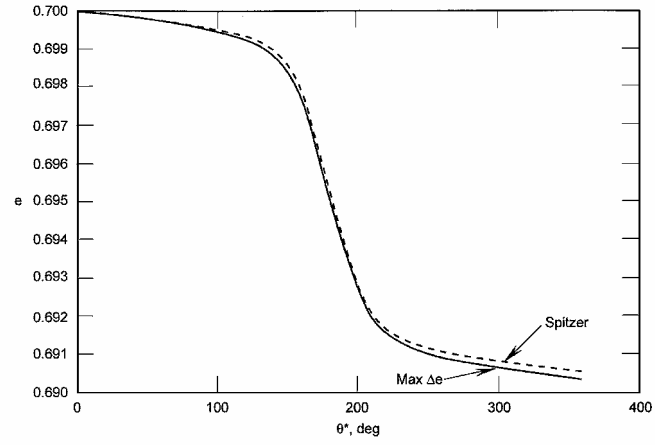

Fig. 13 Eccentricity variation for maximum Δe and Spitzer[4,5] solutions for $a_0 = 40{,}000$ km and $e_0 = 0.7$ elliptic orbit without shadow arc.

The fully coupled Eqs. (18) and (19) yield $a_f = 39{,}999.9992$ km and $e_f = 0.6904825413$ on integration. The Spitzer[4,5] mode in the absence of any shadow arc yields rather accurate results holding effectively the orbit energy at its initial value and providing almost the largest Δe change possible with the variable α law of the optimal solution. These facts are verified in Figs. 11–13, which show the near similarity of the evolutions of a and e of the Spitzer and the optimal solutions.

Simultaneous Circularization and Orbit Rotation in the Near-Circular Case

The averaged rate of change of the eccentricity using the in-plane Spitzer[4,5] firing mode is rewritten from Eq. (27) as

$$\left(\frac{\widetilde{\mathrm{d}e}}{\mathrm{d}t}\right) = \frac{3}{2}kc_\beta\left(\frac{p}{\mu}\right)^{\frac{1}{2}} \tag{35}$$

where k has been replaced by kc_β, the in-plane thrust acceleration, with β the out-of-plane thrust angle or the angle between the thrust vector and its projection onto the orbit plane. An averaged rate for the inclination is also easily constructed from the exact rate of change $\mathrm{d}i/\mathrm{d}t$ valid in near-circular orbit:

$$\frac{\mathrm{d}i}{\mathrm{d}t} = \frac{r}{(\mu p)^{\frac{1}{2}}}\cos(\omega+\theta^*)f_h \cong \frac{1}{(\mu/a)^{\frac{1}{2}}}\cos(\omega+\theta^*)f_h$$

$$\left(\frac{\widetilde{\mathrm{d}i}}{\mathrm{d}t}\right) = \frac{ks_\beta}{(\mu/a)^{\frac{1}{2}}}\frac{1}{2\pi}\times 2\int_{-\pi/2}^{\pi/2} c_{\theta^*}\,\mathrm{d}\theta^*$$

$$\left(\frac{\widetilde{\mathrm{d}i}}{\mathrm{d}t}\right) = \frac{2}{\pi}\frac{ks_\beta}{(\mu/a)^{\frac{1}{2}}} \tag{36}$$

where the out-of-plane acceleration f_h is written as ks_β and where $\omega = 0$ for convenience. This form can also be arrived at by writing $(\mathrm{d}i/\mathrm{d}E)$ as $[(\mathrm{d}i/\mathrm{d}t)/(\mathrm{d}E/\mathrm{d}t)]$ and integrating between the appropriate bounds to generate an expression for Δi, which is then divided by $2\pi/n$ to give the averaged rate such as in Ref. 6. We can now obtain an expression for the constant out-of-plane angle β by forming $(\widetilde{\mathrm{d}i/\mathrm{d}e})$:

$$\left(\frac{\widetilde{\mathrm{d}i}}{\mathrm{d}e}\right) = \left(\frac{\widetilde{\mathrm{d}i}}{\mathrm{d}t}\right) \Big/ \left(\frac{\widetilde{\mathrm{d}e}}{\mathrm{d}t}\right) = \frac{4}{3\pi}\frac{\tan\beta}{(1-e^2)^{\frac{1}{2}}}$$

such that

$$\int_{i_0}^{i} \mathrm{d}i = \frac{4}{3\pi}\tan\beta \int_{e_0}^{e} \frac{\mathrm{d}e}{(1-e^2)^{\frac{1}{2}}}$$

or

$$(i - i_0) = (4/3\pi)\tan\beta\left(\sin^{-1} e - \sin^{-1} e_0\right)$$

and finally,

$$\tan\beta = \frac{(3\pi/4)(i - i_0)}{\left(\sin^{-1} e - \sin^{-1} e_0\right)} \tag{37}$$

This expression can also be obtained from Eq. (28) written as

$$\sin^{-1} e - \sin^{-1} e_0 = \tfrac{3}{2}(a/\mu)^{\frac{1}{2}} k c_\beta t_f \tag{38}$$

and Eq. (36), which gives on integration

$$\Delta i = i - i_0 = (2/\pi)(a/\mu)^{\frac{1}{2}} k s_\beta t_f \tag{39}$$

Replacing t_f from Eq. (39) into Eq. (38) yields Eq. (37), which is now used to yield

$$s_\beta = \frac{\frac{3}{4}\pi(i - i_0)}{\left[\left(\sin^{-1} e - \sin^{-1} e_0\right)^2 + (9/16)\pi^2(i - i_0)^2\right]^{\frac{1}{2}}}$$

This expression of s_β is inserted in Eq. (39) yielding the transfer time t_f, which gives the velocity change

$$\Delta V = k t_f = \tfrac{2}{3}(\mu/a)^{\frac{1}{2}}\left[\left(\sin^{-1} e - \sin^{-1} e_0\right)^2 + (9/16)\pi^2(i - i_0)^2\right]^{\frac{1}{2}} \tag{40}$$

Conclusions

The maximization of the change in the semimajor axis subject to the constraint of zero change in the eccentricity has been extended to the dual problem of maximizing the change in the eccentricity subject to zero change in the semimajor axis, in the near-circular discontinuous thrust case over a single revolution. The solution is obtained by direct application of the theory of the maxima and minima and through a numerical search for the value of the appropriate constant Lagrange multiplier such that a certain integral is driven to zero. The analysis has also been extended to the general elliptic case using continuous thrust and compared with Spitzer's[4,5] simple scheme of applying the thrust vector normal to the orbit line of apsides. When this latter firing mode is used, analytic expressions for the current value of the eccentricity and the accumulated velocity change are derived for the circularization problem.

The use of the Spitzer[4,5] scheme in the presence of a shadow arc leads to an important change in the semimajor axis that can only be effectively constrained with the use of the optimal solution described in this paper.

Finally, simple expressions for the constant out-of-plane thrust angle as well as the total required velocity change to circularize and rotate simultaneously a near-circular orbit are also derived analytically for preliminary analyses.

Acknowledgment

This paper was presented at the 2nd International Symposium on Low Thrust Trajectories, Centre Spatial de Toulouse, Toulouse, France, 18–20 June 2002.

References

[1] Edelbaum, T. N., "Propulsion Requirements for Controllable Satellites," *ARS Journal*, Aug. 1961, pp. 1079–1089.

[2] Cass, J. R., "Discontinuous Low Thrust Orbit Transfer," M.S. Thesis, School of Engineering, U.S. Air Force Inst. of Technology, Rept. AFIT/GA/AA/83D-1, Wright–Patterson AFB, OH, Dec. 1983.

[3] Kéchichian, J. A., "Low-Thrust Eccentricity-Constrained Orbit Raising," *Journal of Spacecraft and Rockets*, Vol. 35, No. 3, 1998, pp. 327–335.

[4] Spitzer, A., "Near Optimal Transfer Orbit Trajectory Using Electric Propulsion," American Astronautical Society, AAS Paper 95-215, Feb. 1995.

[5] Spitzer, A., "Novel Orbit Raising Strategy Makes Low Thrust Commercially Viable," 24th International Electric Propulsion Conf., IEPC Paper 95-212, Sept. 1995.

[6] Burt, E. G. C., "On Space Maneuvers with Continuous Thrust," *Planetary and Space Science*, Vol. 15, 1967, pp. 103–122.

D. B. Spencer
Associate Editor